Circuits Syst Signal Process (2018) 37:3702–3724
https://doi.org/10.1007/s00034-018-0750-7

Hyperchaotic Memcapacitor Oscillator with Infinite Equilibria and Coexisting Attractors

Karthikeyan Rajagopal[1,2] · **Sajad Jafari**[3] · **Anitha Karthikeyan**[1,2] · **Ashokkumar Srinivasan**[2] · **Biniyam Ayele**[2]

Received: 3 April 2017 / Revised: 30 December 2017 / Accepted: 5 January 2018 /
Published online: 20 January 2018
© Springer Science+Business Media, LLC, part of Springer Nature 2018

Abstract A newly introduced charge-controlled memcapacitor-based hyperchaotic oscillator with coexisting chaotic attractors is investigated. Dynamic analysis of the oscillator shows that it has infinite number of equilibrium points and shows multistability. Its multistability analysis in the parameter space shows the existence of chaotic and hyperchaotic attractors. Fractional-order analysis of the hyperchaotic oscillator shows that the hyperchaos remains in the fractional order too. Field programmable gate arrays are used to realize the proposed oscillator.

Keywords Memcapacitor · Hyperchaos · Multistability · Fractional order · FPGA

✉ Karthikeyan Rajagopal
rkarthiekeyan@gmail.com

Sajad Jafari
sajadjafari83@gmail.com

Anitha Karthikeyan
Mrs.anithakarthikeyan@gmail.com

Ashokkumar Srinivasan
Sashok06@gmail.com

Biniyam Ayele
biniyamayeledec@gmail.com

1 Department of Electrical and Communication Engineering, Center for Nonlinear Dynamics, The PNG University of Technology, Lae, Papua New Guinea

2 Center for Nonlinear Dynamics, Defence University, Bishoftu, Ethiopia

3 Biomedical Engineering Department, Amirkabir University of Technology, Tehran, Iran

1 Introduction

The fourth circuit element popularly known as memristors was first postulated by Chua [15]. Until 2008 when researchers of HP laboratories fabricated a solid-state implementation of memristor, there were not many works on memristor realization [67]. Then, many other memristor models have been introduced [5,8,10,16]. Memristors are considered to be highly nonlinear with nonvolatile characteristics and can be implemented with nanoscale technologies [5,8,10,16]. To design memristor oscillators, a new kind of nonlinear circuits with oscillatory memories and periodically forced flux controlled memductance models are investigated [32,47].

Memristor-based chaotic oscillators are widely investigated in the recent years. Circuits with two HP memristors in antiparallel have been demonstrated showing a variety of chaotic attractors for different values of components [11]. A current feedback op-amp-based memristor oscillators has been analyzed, and simulation results have been investigated [54]. A simple autonomous memristor-based oscillator with external sinusoidal excitation has been used to generate chaotic oscillations. A discrete model for this HP memristor has been derived and implemented using DSP chips [76] implementing memristor. Recently, a new hyperchaotic system with two memristors has been investigated and its application to image encryption has been analyzed.

Practical implementation of memristor-based chaotic circuits with off-the-shelf components is desired for real-time applications [46]. Memristor-based chaotic circuit for pseudorandom number generation has been analyzed with applications to cryptography [18]. Memristor-based chaotic circuits for text and image cryptography have been investigated, and the correlation analysis shows the effectiveness of the proposed cryptographic scheme over other encryption algorithms [82]. Memcapacitor-based chaotic circuits with a HP memristor have been proposed and implemented in DSP for further applications [77].

Recently, many researchers have discussed about fractional-order calculus and its applications [3,22,38]. Fractional-order nonlinear systems with different control approaches have been investigated in [2,9,84]. Fractional-order memristor-based no equilibrium chaotic and hyperchaotic systems have been proposed [55–58]. A novel fractional-order no equilibrium chaotic system has been investigated in [43], and a fractional-order hyperchaotic system without equilibrium points has been investigated in [12]. Memristor-based fractional-order system with a capacitor and an inductor has been discussed [21]. Numerical analysis and methods for simulating fractional-order nonlinear system have been proposed in [49], and MATLAB solutions for fractional-order chaotic systems have been discussed in [74].

Implementation of chaotic and hyperchaotic systems using field programmable gate arrays (FPGA) have been widely investigated [23,72,79]. Chaotic random number generators have been implemented in FPGA for applications in image cryptography [71]. A FPGA-implemented Duffing oscillator-based signal detector has been proposed [59]. Digital implementations of chaotic multiscroll attractors have been extensively investigated [72,73]. Memristor-based chaotic system and its FPGA circuit have been discussed with their qualitative analysis [81]. A FPGA implementation of fractional-order chaotic system using approximation method has been investigated recently for the first time [55–58].

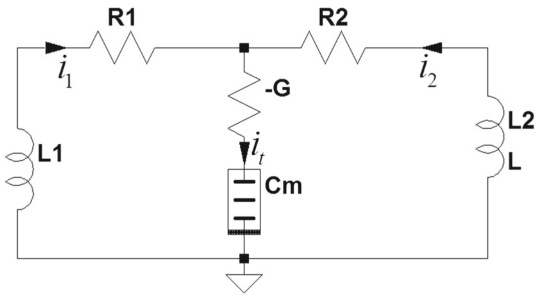

Fig. 1 Memcapacitor-based hyperchaotic oscillator

In this paper, we investigate the dynamical properties of a memcapacitor chaotic oscillator [51] and derive and analyze its fractional-order model. The entire paper is organized into eight sections with Sect. 1 giving the introduction and Sect. 7 the conclusion part. In the second section, we derive the dynamical dimensionless model of the memcapacitor oscillator. In the Sect. 3, we discuss the various dynamical properties of the oscillator like dissipativity, stability of equilibrium, Lyapunov exponents, bifurcation and bicoherence. In Sect. 4, we derive the dimensionless fractional-order model of the proposed memcapacitor oscillator and Sect. 5 deals with its dynamical analysis. In Sect. 6, we implement the fractional-order memcapacitor oscillator in field programmable gate arrays (FPGA).

2 Problem Formulation

Several memcapacitor models, including piecewise linear, quadric and cubic function models, memristor-based memcapacitor models have been discussed in several literatures [26,48,75,83]. Some special phenomena such as hidden attractors [19,20,24,36, 40] and coexistence attractors [7,17,44,62] have been found in memcapacitor-based chaotic oscillators.

In this paper, we investigate the memcapacitor-based hyperchaotic oscillator discussed in [78] as shown in Fig. 1. The multistability of the proposed oscillator is discussed with the parameter space of the system rather than the initial conditions as discussed in [78].

In this circuit, R_1, R_2 are the resistances, L_1, L_2 are the inductances, and G is the conductance. C_{m} is the memcapacitor as discussed in [77]. The current flowing through the circuit is i_1, i_2. Applying Kirchhoff's current law to the circuit shown in Fig. 1, the change in flux is defined as

$$\frac{\mathrm{d}q_{C_{\mathrm{m}}}}{\mathrm{d}t} = i_1 + i_2 \tag{1}$$

where $q_{C_{\mathrm{m}}}$ is the charge through the memcapacitor. The current through the inductor L_1 is derived as,

$$\frac{\mathrm{d}i_1}{\mathrm{d}t} = \frac{1}{L_1}\left[-V_{C_{\mathrm{m}}} - i_1 R_1 + (i_1 + i_2)\, R_0\right] \tag{2}$$

and the current through the inductor L_2 is defined as,

$$\frac{\mathrm{d}i_2}{\mathrm{d}t} = \frac{1}{L_2}\left[-V_{C_\mathrm{m}} - i_2 R_2 + (i_1 + i_2)\, R_0\right] \tag{3}$$

The relationship between the voltage across the memcapacitor $v_{C_\mathrm{M}}(t)$ and the charge $q_{C_\mathrm{m}}(t)$ of the memcapacitor is defined as,

$$v_{C_\mathrm{M}}(t) = (\alpha + \beta\sigma^2) q_{C_\mathrm{m}}(t) \tag{4}$$

where $\alpha + \beta\sigma^2$ is the inverse memcapacitance and σ is the time integral of charge $q_{C_\mathrm{m}}(t)$ given by $\sigma = \int_{t_0}^{t} q_{C_\mathrm{m}}(t)$. Using Eqs. (2), (3), and (4), a fourth-order Memcapacitor system is derived as below,

$$\begin{aligned}
\tfrac{\mathrm{d}q_{C_\mathrm{m}}}{\mathrm{d}t} &= i_1 + i_2 \\
\tfrac{\mathrm{d}i_1}{\mathrm{d}t} &= \tfrac{1}{L_1}\left[-(\alpha + \beta\sigma^2) q_{C_\mathrm{m}}(t) - i_1 R_1 + (i_1 + i_2)\, R_0\right] \\
\tfrac{\mathrm{d}i_2}{\mathrm{d}t} &= \tfrac{1}{L_2}\left[-(\alpha + \beta\sigma^2) q_{C_\mathrm{m}}(t) - i_2 R_2 + (i_1 + i_2)\, R_0\right] \\
\tfrac{\mathrm{d}\sigma}{\mathrm{d}t} &= q_{C_\mathrm{m}}(t)
\end{aligned} \tag{5}$$

where $q_{C_\mathrm{m}}(t)$ is the charge through the memcapacitor, i_1 and i_2 are the circuit currents, v_{C_m} is the memcapacitor voltage, and σ is the integral parameter of the memcapacitor charge.

To derive a generalized 4D model, let us define $x = q_{C_\mathrm{m}}(t)$, $y = i_1, z = i_2, w = \sigma$ and the parameters as $a = \frac{\alpha}{L_1}, b = \frac{\beta}{L_1}, c = \frac{(R_0 - R_1)}{L_1}, d = \frac{R_0}{L_1}, f = \frac{R_0}{L_2}, e = \frac{(R_0 - R_2)}{L_1}, m = \frac{\alpha}{L_2}, n = \frac{\beta}{L_2}$.

By applying the assumptions in the derived Eq. (5), we arrive at the 4D dimensionless mathematical model of the memcapacitor system as,

$$\begin{aligned}
\tfrac{\mathrm{d}x}{\mathrm{d}t} &= y + z \\
\tfrac{\mathrm{d}y}{\mathrm{d}t} &= cy + dz - ax - bxw^2 \\
\tfrac{\mathrm{d}z}{\mathrm{d}t} &= fy + ez - mx - nxw^2 \\
\tfrac{\mathrm{d}w}{\mathrm{d}t} &= x
\end{aligned} \tag{6}$$

The parameters of the above equation for which the system exhibits hyperchaotic oscillations are, $a = 5.8, b = 2, c = 2.6, d = 0.1, e = -3.4, f = 0.2, m = 2.8, n = 6.8$. The initial conditions are chosen as $(0.001, 0.001, 0.01, 0.01)$. Figure 2 shows the 2D projections of the strange attractor of system (6).

3 Dynamic Analysis of Hyperchaotic Memcapacitor Oscillator (HMCO)

The dynamic properties of the HMCO system such as dissipativity, equilibrium points, eigenvalues, Lyapunov exponents and Kaplan–Yorke dimension are derived and discussed in this section.

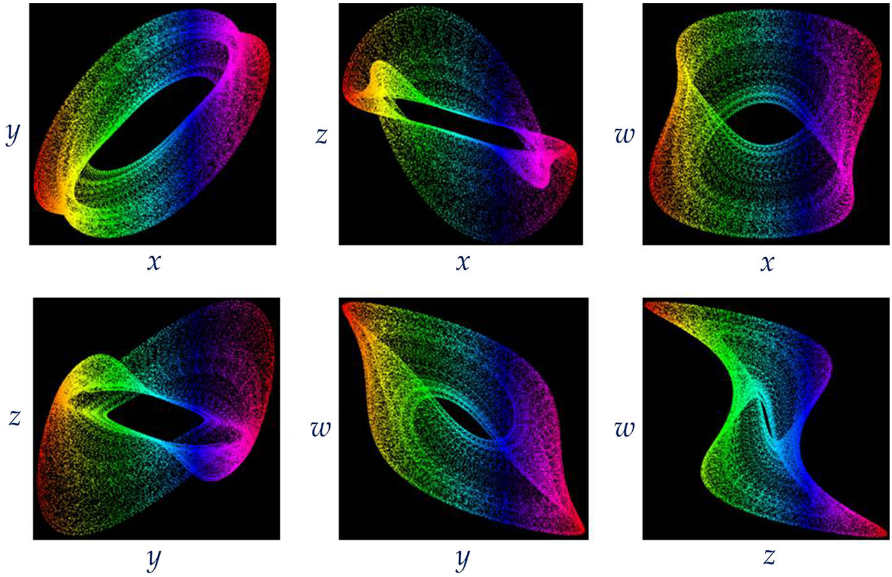

Fig. 2 2D projections of the strange attractor of system (6)

3.1 Dissipativity

In vector notation, the 4-D system (6) can be expressed as

$$\dot{X} = f(X) = \begin{bmatrix} f_1(x, y, z, w) \\ f_2(x, y, z, w) \\ f_3(x, y, z, w) \\ f_4(x, y, z, w) \end{bmatrix} \tag{7}$$

where

$$\begin{cases} f_1(x, y, z, w) = y + z \\ f_2(x, y, z, w) = cy + dz - ax - bxw^2 \\ f_3(x, y, z, w) = fy + ez - mx - nxw^2 \\ f_4(x, y, z, w) = x \end{cases} \tag{8}$$

Let Ω be any region in R^4 with a smooth boundary and also, $\Phi(t) = \Phi_t(\Omega)$, where Φ_t is the flow of the vector field f. Furthermore, let $V(t)$ denote the hyper volume of $\Phi(t)$.

By Liouville's theorem, we have

$$\dot{V} = \int_{\Phi(t)} (\nabla \cdot f)\mathrm{d}x\mathrm{d}y\mathrm{d}z\mathrm{d}w \tag{9}$$

The divergence of the vector field f is easily calculated as

$$\nabla \cdot f = \frac{\partial f_1}{\partial x} + \frac{\partial f_2}{\partial y} + \frac{\partial f_3}{\partial z} + \frac{\partial f_4}{\partial w} = c + e = -0.8 \leq 0 \tag{10}$$

Substituting (10) into (9), we obtain the first-order differential equation

$$\dot{V}(t) = -0.8V(t) \tag{11}$$

Integrating (11), we obtain the unique solution as

$$V(t) = \exp(-0.8t)V(0) \text{ for all } t \geq 0 \tag{12}$$

It follows that $V(t) \to 0$ exponentially as $t \to \infty$. This shows that the HMCO system (6) is dissipative.

3.2 Equilibrium Points

By equating $\dot{X} = 0$, the HMCO system (6) shows three equations $y+z = 0$, $cy+dz = 0$ and $fy + ez = 0$. As c, d, f, e are all positive the first possible solution for the equations are $y = -\rho_1, z = \rho_1$ for $c = d$, $f = e$ and the corresponding equilibrium set is $[0, -\rho_1, \rho_1, \rho_2]$ and the second possible solution is $y = z = 0$ for $c \neq d$, $f \neq e$ and the corresponding equilibrium set is $[0, 0, 0, \rho_3]$ where ρ_1, ρ_2, ρ_3 are arbitrary constants. Thus, the HMCO system has infinite number of equilibrium points located on a line (similar to the systems proposed in [4,29,30,33,51,52]) with two possible equilibrium sets.

The Jacobian matrix of the HMCO system (6) for $c = d$, $f = e$ or $c \neq d$, $f \neq e$ is found as

$$J(X) = \begin{bmatrix} 0 & 1 & 1 & 0 \\ -a - b\rho_{2,3}^2 & c & d & 0 \\ -m - n\rho_{2,3}^2 & f & e & 0 \\ 1 & 0 & 0 & 0 \end{bmatrix} \tag{13}$$

The constants ρ_2, ρ_3 have same effect on the system. The characteristic equation of the system is derived as,

$$\lambda^4 - (c+e)\lambda^3 + \begin{pmatrix} a + m + ce - df \\ +b\rho_{2,3}^2 + n\rho_{2,3}^2 \end{pmatrix} \lambda^2 + \begin{pmatrix} af - ae - cm + dm \\ +dn\rho_{2,3}^2 - be\rho_{2,3}^2 \\ +bf\rho_{2,3}^2 - cn\rho_{2,3}^2 \end{pmatrix} \lambda \tag{14}$$

As per Routh–Hurwitz criterion, all the principal minors need to be positive in order to having stable equilibrium. The principal minors are,

$$\Delta_1 = \delta_1 > 0,\ \Delta_2 = \begin{vmatrix} \delta_1 & \delta_0 \\ \delta_3 & \delta_2 \end{vmatrix} > 0,\ \Delta_3 => \begin{vmatrix} \delta_1 & \delta_0 & 0 \\ \delta_3 & \delta_2 & \delta_1 \\ 0 & \delta_4 & \delta_3 \end{vmatrix} > 0,$$

$$\Delta_4 = \begin{vmatrix} \delta_1 & \delta_0 & 0 & 0 \\ \delta_3 & \delta_2 & \delta_1 & \delta_0 \\ 0 & \delta_4 & \delta_3 & \delta_2 \\ 0 & 0 & 0 & \delta_4 \end{vmatrix} > 0$$

where

$$\delta_0 = 1, \delta_1 = -(c+e), \delta_2 = a + m + ce - df + b\rho_{2,3}^2 + n\rho_{2,3}^2$$
$$\delta_3 = af - ae - cm + dm + dn\rho_{2,3}^2 - be\rho_{2,3}^2 + bf\rho_{2,3}^2 - cn\rho_{2,3}^2, \delta_4 = 0$$

For the parameter values of $a = 5.8, b = 2, c = 2.6, d = 0.1, e = -3.4, f = 0.2, m = 2.8, n = 6.8$, the equilibrium is unstable and the system shows chaotic oscillations when the arbitrary constant $\rho_{2,3}$ lies between the range $[-1.5, 1.5]$ as discussed in [78].

3.3 Lyapunov Exponents and Kaplan–Yorke Dimension

Lyapunov exponents of a nonlinear system define the convergence and divergence of the states. Although there are different methods and important issues about this quantity [6,34,35,37,66], in this work we have used the famous method proposed in [80]. Lyapunov exponents (LEs) are necessary and more convenient for detecting hyperchaos in fractional-order hyperchaotic system. A definition of LEs for fractional differential systems was given in [41] based on frequency-domain approximations, but the limitations of frequency-domain approximations are highlighted in [70]. Time series-based LEs calculation methods like Wolf algorithm [80], Jacobian method [25] and neural network algorithm [45] are popularly known ways of calculating Lyapunov exponents for integer and fractional-order systems. To calculate the LEs of the HMCO system, we use the Jacobian method.

The Lyapunov exponents of the HMCO system are numerically found as

$$L_1 = 0.2991, L_2 = 0.07634, L_3 = 0, L_4 = -1.0741 \tag{15}$$

Since there are two positive Lyapunov exponents in (15), it is clear that the HMCO system (6) is hyperchaotic (Fig. 3).

We note that the sum of the Lyapunov exponents of the HMCO system (6) is negative. In fact,

$$L_1 + L_2 + L_3 + L_4 = -0.6987 < 0 \tag{16}$$

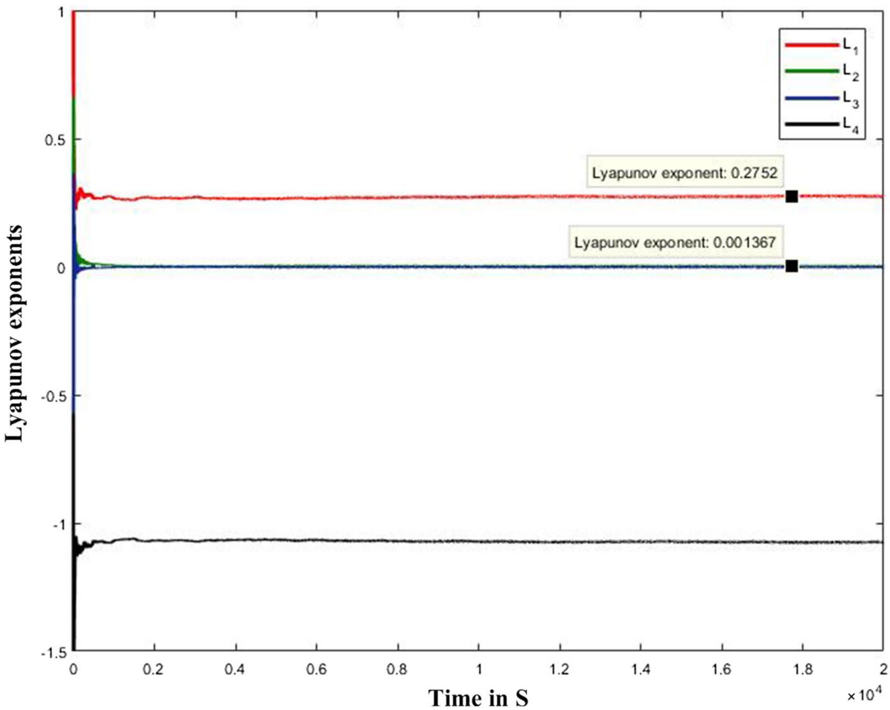

Fig. 3 Lyapunov exponents of the HMCO system for $a = 5.8$, $b = 2$, $c = 2.6$, $d = 0.1$, $e = -3.4$, $f = 0.2$, $m = 2.8$, $n = 6.8$ and initial conditions $(0.001, 0.001, 0.01, 0.01)$

This shows that the HMCO system (6) is dissipative.

Also, the Kaplan–Yorke dimension of the HMCO system (6) is derived as

$$D_{KY} = 3 + \frac{L_1 + L_2 + L_3}{|L_4|} = 3.3495, \tag{17}$$

which is fractional.

3.4 Bifurcation and Multistability in the HMCO System

Multistability possesses a threat for engineering systems because of its unpredicted behavior [17]. Many chaotic systems have shown multistability and coexisting attractors [28,64,65,69]. Multistability analysis of symmetric Rossler system with amplitude controls provides good idea about multistability generates from the symmetrization [42]. Multistability in hidden attractor systems and control of multistability through the scheme of linear augmentation that can drive multistability to mono stability has been investigated [61]. Multistability in large system of the coupled pendula is investigated in [31]. The occurrence of multiheading chimera states of the coupled pendula which can create different types of synchronous states has been also discussed [31].

The HMCO system shows multistability as can be seen from Fig. 4 which shows the evidence of discontinuous bifurcations. The bifurcation diagram is obtained by plotting local maxima of the coordinate y in terms of the parameter d that is increased (or decreased) in tiny steps. The final state at each iteration of the parameter serves as the initial state for the next iteration. This strategy, known as forward and backward continuation, represents a simple way to localize the window in which the system develops multistability [63]. The existence of multistability can be confirmed by comparing the forward (dark blue color) and backward (red color) bifurcation diagrams as shown in Fig. 4a. Figure 4b shows the coexisting multiple attractors of the HMCO system for $d = 0.5$ and various initial conditions.

3.5 Bicoherence

Higher-order spectra have been used to study the nonlinear interactions between frequency modes [39,53]. Let $x(t)$ be a stationary random process defined as,

$$x(t) = \sum_{n=1}^{N} A_n e^{j\omega_n t} + A_n^* e^{-j\omega_n t} \tag{18}$$

where ω is the angular frequency, n is the frequency modal index, and A_n are the complex Fourier coefficients. The power spectrum can be defined as,

$$P(\omega_k) = E[A_{\omega_k} A_{\omega_k}^*] \tag{19}$$

and discrete bispectrum can be defined as,

$$B(\omega_k, \omega_j) = E[A_{\omega_k} A_{\omega_j} A_{\omega_k+\omega_j}^*] \tag{20}$$

If the modes are independent, then the average triple products of Fourier components are zero resulting in a zero bispectrum [39]. The study of bicoherence is to give an indication of the relative degree of phase coupling between triads of frequency components. The motivation to study the bicoherence is twofold. First, the bicoherence can be used to extract information due to deviations from Gaussianity and suppress additive (colored) Gaussian noise. Second, the bicoherence can be used to detect and characterize asymmetric nonlinearity in signals via quadratic phase coupling or identify systems with quadratic nonlinearity. The bicoherence is the third-order spectrum. Whereas the power spectrum is a second-order statistics, formed from $X'(f) * X(f)$, where $X(f)$ is the Fourier transform of $x(t)$, the bispectrum is a third-order statistics formed from $X(f_j) * X(f_k) * X'(f_j + f_k)$. The bispectrum is therefore a function of a pair of frequencies (f_j, f_k) . It is also a complex-valued function. The (normalized) square amplitude is called the bicoherence (by analogy with the coherence from the cross-spectrum).The bispectrum is calculated by dividing the time series into M segments of length N_seg, calculating their Fourier transforms and bi-periodogram, then averaging over the ensemble. Although the bicoherence is a function of two frequencies, the default output of this function is a one dimensional output, the bicoherence

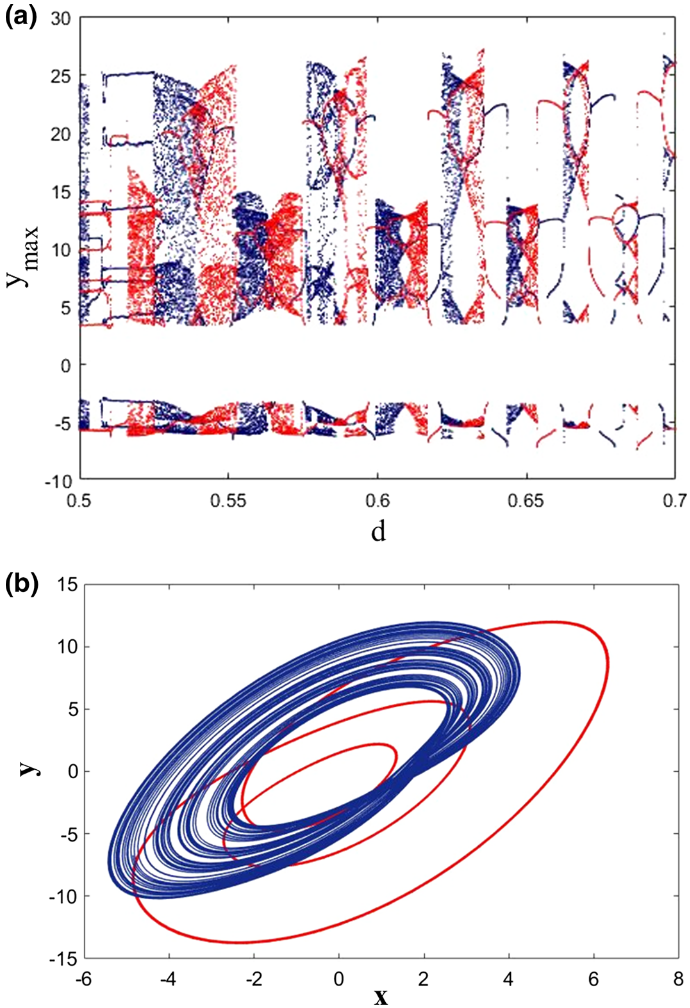

Fig. 4 **a** Bifurcation of HMCO system for parameter d (forward continuation in dark blue color and backward continuation in red color). **b** Coexisting attractors of the HMCO system for $d = 0.5$ at initial conditions [1, 1, 0.1, 1] (red plot), [1, 1, 1, 1] (green plot), [0.8, 0.01, 0.01, 0.01] (blue plot) (Color figure online)

refined as a function of only the sum of the two frequencies. The auto-bispectrum of a chaotic system is given by Pezeshki [50]. He derived the auto-bispectrum with the Fourier coefficients.

$$B(\omega_1, \omega_2) = E[A(\omega_1)A(\omega_2)A^*(\omega_1 + \omega_2)] \tag{21}$$

where ω_n is the radian frequency and A is the Fourier coefficients of the time series. The normalized magnitude spectrum of the bispectrum known as the squared bicoherence is given by

$$b(\omega_1, \omega_2) = |B(\omega_1, \omega_2)|^2 / P(\omega_1) P(\omega_2) P(\omega_1 + \omega_2) \tag{22}$$

where $P(\omega_1)$ and $P(\omega_2)$ are the power spectrums at f_1 and f_2.

Figure 5 shows the bicoherence contours of the FOHMCO system for state x and all states together, respectively. Shades in yellow represent the multifrequency components contributing to the power spectrum. From Fig. 5, the cross-bicoherence is significantly nonzero, and non-constant, indicating a nonlinear relationship between the states. As can be seen from Fig. 5a, the spectral power is very low as compared to the spectral power of all states together (Fig. 5b) indicating the existence of multifrequency nodes. Also Fig. 5b shows the nonlinear coupling (straight lines connecting multiple frequency terms) between the states. The yellow shades/lines and non-sharpness of the peaks, as well as the presence of structure around the origin in figures (cross-bicoherence), indicates that the nonlinearity between the states x, y, z, w is not of the quadratic nonlinearity and hence may be because of nonlinearity of higher dimensions. The most two dominant frequencies (f_1, f_2) are taken for deriving the contour of bicoherence. The sampling frequency (f_s) is taken as the reference frequency. Direct FFT is used to derive the power spectrum for individual frequencies, and Hankel operator is used as the frequency mask. Hanning window is used as the FIR filter to separate the frequencies [60].

4 Fractional-Order HMCO System (FOHMCO)

In this section, we derive the fractional-order model of the hyperchaotic memcapacitor oscillator (FOHMCO). There are three commonly used definition of the fractional-order differential operator, *viz.* Grunwald–Letnikov, Riemann–Liouville and Caputo [3,22,38].

We use the Grunwald–Letnikov (GL) definition, which is defined as

$$\begin{aligned} {}_aD_t^q f(t) &= \lim_{h \to 0} \left\{ \frac{1}{h^q} \sum_{j=0}^{\left[\frac{t-q}{h}\right]} (-1)^j \binom{q}{j} f(t - jh) \right\} \\ &= \lim_{h \to 0} \left\{ \frac{1}{h^q} \Delta_h^q f(t) \right\} \end{aligned} \tag{23}$$

where a and t are limits of the fractional-order equation, $\Delta_h^q f(t)$ is generalized difference, h is the step size, and q is the fractional-order of the differential equation.

For numerical calculations, the above equation is modified as

$${}_{(t-L)}D_t^q f(t) = \lim_{h \to 0} \left\{ h^{-q} \sum_{j=0}^{N(t)} b_j \left(f(t - jh) \right) \right\} \tag{24}$$

Theoretically fractional-order differential equations use infinite memory. Hence, when we want to numerically calculate or simulate the fractional-order equations we have to

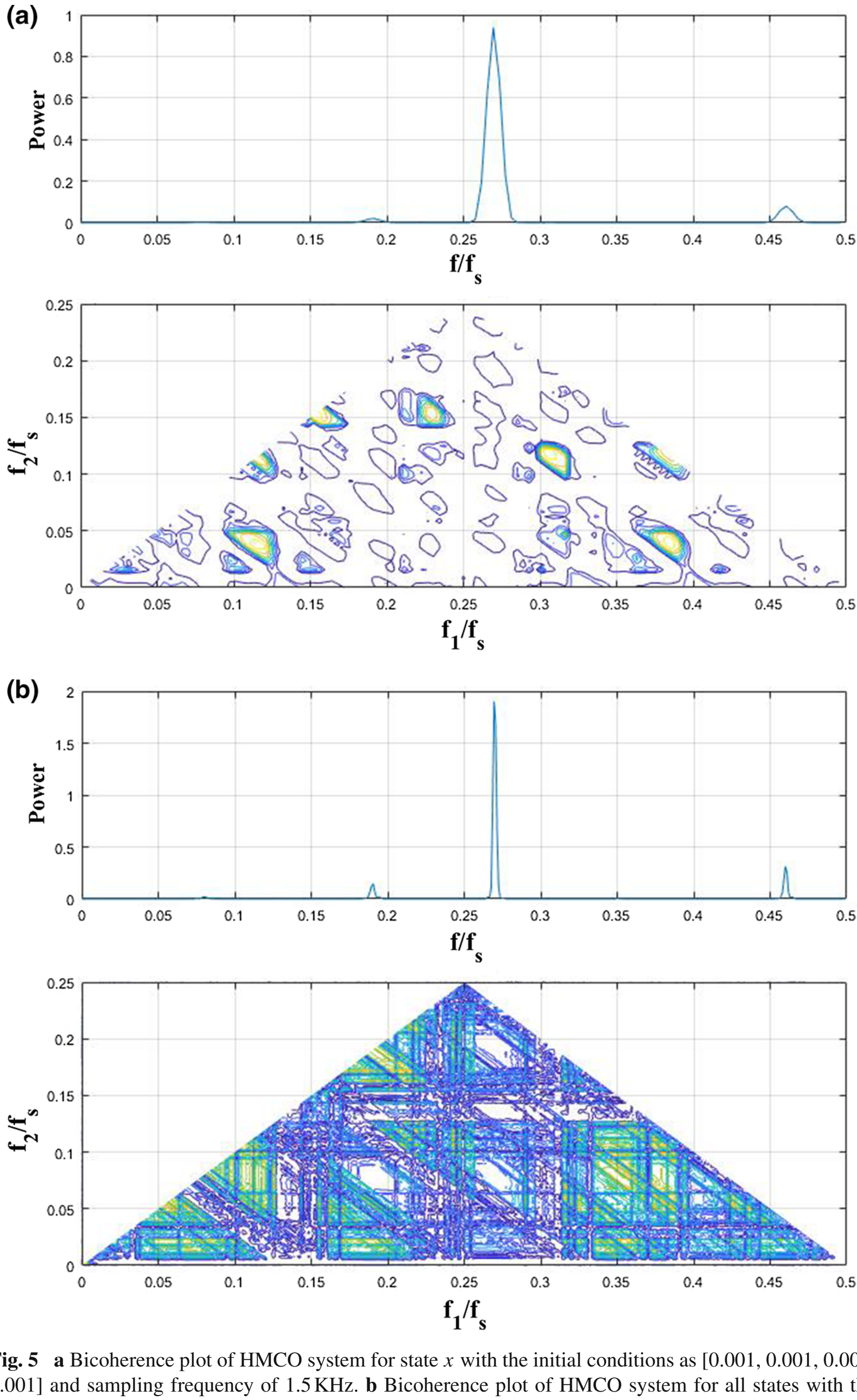

Fig. 5 **a** Bicoherence plot of HMCO system for state x with the initial conditions as [0.001, 0.001, 0.001, 0.001] and sampling frequency of 1.5 KHz. **b** Bicoherence plot of HMCO system for all states with the initial conditions as [0.001, 0.001, 0.001, 0.001] and sampling frequency of 1.5 KHz

use finite memory principal, where L is the memory length and h is the time sampling.

$$N(t) = \min\left\{\left[\frac{t}{h}\right], \left[\frac{L}{h}\right]\right\} \tag{25}$$

The binomial coefficients required for the numerical simulation are calculated as,

$$b_j = \left(1 - \frac{a+q}{j}\right) b_{j-1} \tag{26}$$

Using (23)–(26), the FOHMCO system is derived as,

$$\begin{aligned} \frac{\mathrm{d}^{q_x} x}{\mathrm{d}t^{q_x}} &= y + z \\ \frac{\mathrm{d}^{q_y} y}{\mathrm{d}t^{q_y}} &= cy + dz - ax - bxw^2 \\ \frac{\mathrm{d}^{q_z} z}{\mathrm{d}t^{q_z}} &= fy + ez - mx - nxw^2 \\ \frac{\mathrm{d}^{q_w} w}{\mathrm{d}t^{q_w}} &= x \end{aligned} \tag{27}$$

where q_x, q_y, q_z, q_w are the fractional orders of the FOHMCO system. Figure 6 shows the 2D phase portraits of the FOHMCO system with the same parameter and initial conditions as discussed in Sect. 2.

5 Dynamic Analysis of the FOHMCO Chaotic Systems

5.1 Bifurcation with Fractional Order

Most of the dynamic properties of the HMCO chaotic systems like the Lyapunov exponents and bifurcation with parameters are preserved in the FOHMCO system [55,58] if $q_i > 0.992$ where $i = x, y, z, w$. As can be seen from Fig. 7a, bifurcation of the FOHMCO system for change in fractional order shows that the systems chaotic oscillations remains if $q_i > 0.992$. Based on our calculations, the system shows hyperchaotic behavior for $0.993 \le q \le 0.998$ and positive Lyapunov exponents ($L_1 = 0.3166, L_2 = 0.08217$) of the FOHMCO system appears when $q = 0.998$ against its largest integer-order Lyapunov exponents ($L_1 = 0.2991, L_2 = 0.07634$). Figure 7b–g shows the 2D phase portraits in *Y*–*Z* plane for various fractional orders.

5.2 Stability Analysis

Commensurate Order: For commensurate FOHMCO system of order q, the system is stable and exhibits chaotic oscillations if $|\arg(\mathrm{eig}(J_{\mathrm{E}}))| = |\arg(\lambda_i)| > \frac{q\pi}{2}$ where J_{E} is the Jacobian matrix at the equilibrium E and λ_i are the eigenvalues of the FOHMCO system where $i = 1, 2, 3, 4$. As seen from the FOHMCO system, the eigenvalues should remain in the unstable region and the necessary condition for the FOHMCO system to be stable is $q > \frac{2}{\pi}\tan^{-1}\left(\frac{|\mathrm{Im}\lambda|}{\mathrm{Re}\lambda}\right)$. The HOCM system shows two equilibrium

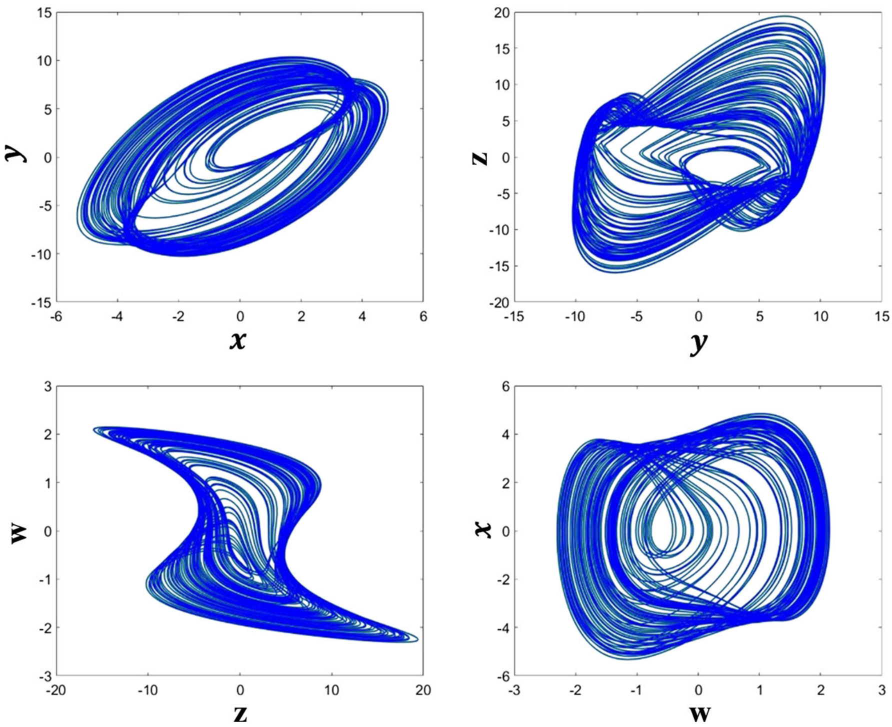

Fig. 6 2D phase portraits of the FOHMCO system for the fractional order $q = 0.998$

sets $y = -\rho_1, z = \rho_1$ for $c = d, f = e$ and the corresponding equilibrium set is $[0, -\rho_1, \rho_1, \rho_2]$ and the second possible solution is $y = z = 0$ for $c \neq d, f \neq e$ and the corresponding equilibrium set is $[0, 0, 0, \rho_3]$ where ρ_1, ρ_2, ρ_3 are the arbitrary constants. For the parameter values discussed in section 2, the FOHOCM system shows stable chaotic oscillations if the arbitrary constant $\rho_{2,3}$ lies in the range $[-1.5, 1.5]$. The characteristic equation of the FOHOCM system for commensurate order is

$$\begin{aligned}
&\lambda^{396} + 4\lambda^{298} + (-c - e)\lambda^{297} + 6\lambda^{200} + (-3c - 3e)\lambda^{199} \\
&\quad + \left(a + m + ce - df + bp23^2 - n\rho_{2,3}^2\right)\lambda^{198} + 4\lambda^{102} \\
&\quad +(-3c - 3e)\lambda^{101} + \left(2a + 2m + 2ce - 2df + 2b\rho_{2,3}^2 + 2n\rho_{2,3}^2\right)\lambda^{100} \\
&\quad + \Big(af - ae - cm + dm + dn\rho_{2,3}^2 \\
&\quad -be\rho_{2,3}^2 + bf\rho_{2,3}^2 - cn\rho_{2,3}^2\Big)\lambda^{99} + \lambda^4 + (-c - e)\lambda^3 \\
&\quad + \left(a + m + ce - df + b\rho_{2,3}^2 + n\rho_{2,3}^2\right)\lambda^2 + \Big(af - ae \\
&\quad -cm + dm + dn\rho_{2,3}^2 - be\rho_{2,3}^2 + bf\rho_{2,3}^2 - cn\rho_{2,3}^2\Big)\lambda
\end{aligned}$$

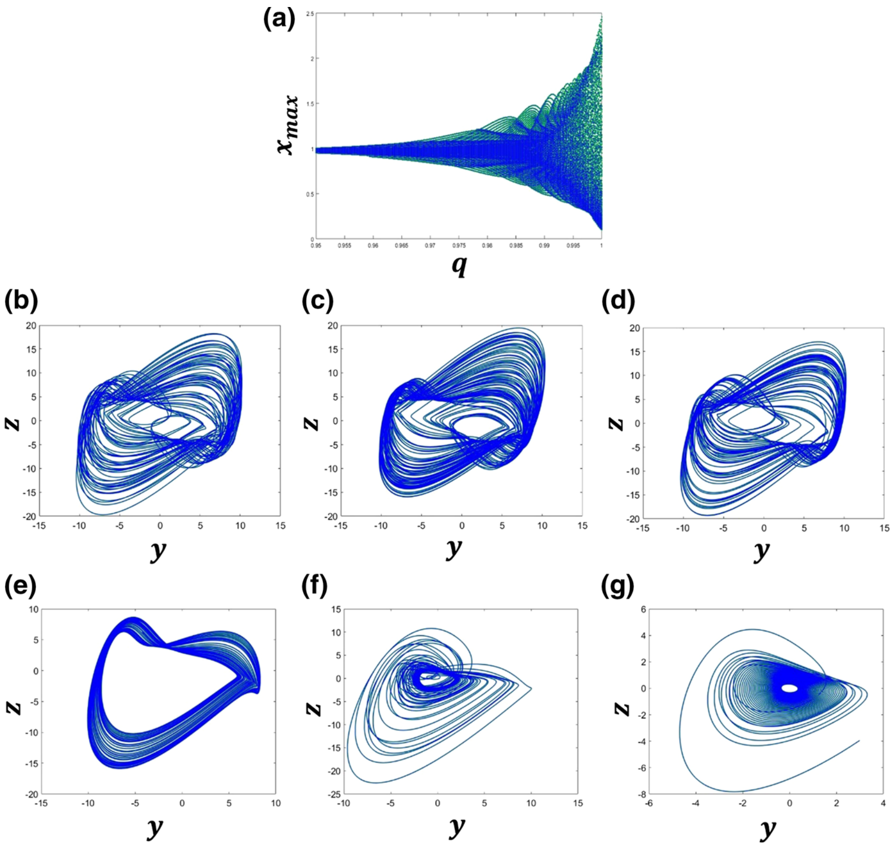

Fig. 7 **a** Fractional-order bifurcation plots and **b**–**g** 2D phase portrait (X–Y plane) of FOHMCO system for various fractional orders (**b** $q = 0.999$, **c** $q = 0.998$, **d** $q = 0.997$, **e** $q = 0.995$, **f** $q = 0.993$, **g** $q = 0.99$)

Incommensurate Order: The necessary condition for the FOHMCO system to exhibit chaotic oscillations in the incommensurate case is, $\frac{\pi}{2M} - \min_i (|\arg(\lambda i)|) > 0$ where M the LCM of the fractional orders. If $q_x = 0.99$, $q_y = 0.99$, $q_z = 0.98$, $q_w = 0.98$, then $M = 100$. The characteristic equation of the system evaluated at the equilibrium is, $\det(\mathrm{diag}[\lambda^{Mq_x}, \lambda^{Mq_y}, \lambda^{Mq_z}, \lambda^{Mq_w}] - J_{\mathrm{E}}) = 0$ and by substituting the values of M and the fractional orders, $\det(diag[\lambda^{99}, \lambda^{99}, \lambda^{98}, \lambda^{98}] - J_{\mathrm{E}}) = 0$ and the characteristic equation is,

$$\begin{aligned}
&\lambda^{394} + 2\lambda^{297} + (2-e)\lambda^{296} - c\lambda^{295} + \lambda^{200} \\
&\quad + (4-e)\lambda^{199} + (1-2e-2c)\lambda^{198} + \left(n\rho_{2,3}^2 - c + m + ce - df\right)\lambda^{197} \\
&\quad + \left(b\rho_{2,3}^2 + a\right)\lambda^{196} + 2\lambda^{102} + (2-2e-c)\lambda^{101} \\
&\quad + \left(n\rho_{2,3}^2 - 2c - e + m + ce - df\right)\lambda^{100} \\
&\quad + \left(2a + m + ce - df + 2b\rho_{2,3}^2 + n\rho_{2,3}^2\right)\lambda^{99}
\end{aligned}$$

$$+\left(af-ae-cm+dm+dn\rho_{2,3}^{2}-be\rho_{2,3}^{2}+bf\rho_{2,3}^{2}-cn\rho_{2,3}^{2}\right)\lambda^{98}$$
$$+\lambda^{4}+(-c-e)\lambda^{3}+\left(a+m+ce-df+b\rho_{2,3}^{2}+n\rho_{2,3}^{2}\right)\lambda^{2}$$
$$+\left(af-ae-cm+dm+dn\rho_{2,3}^{2}-be\rho_{2,3}^{2}+bf\rho_{2,3}^{2}-cn\rho_{2,3}^{2}\right)\lambda$$

For the values of parameters mentioned in Sect. 2 and the value of $\rho_{2,3} = 1$, the approximated solution of the characteristic equation is $\lambda_{394} = 0.977$ and whose argument is zero and which is the minimum argument and hence the stability necessary condition becomes, $\frac{\pi}{20} - 0 > 0$ which solves for $0.0785 > 0$ and hence the FOHMCO system is stable and chaos exists in the incommensurate system.

6 FPGA Implementation of the FOHMCO Systems

In this section, we discuss about the implementation of the proposed FOHMCO systems in FPGA [59,73,81] using the Xilinx (Vivado) System Generator. The three main approaches derived to solve fractional-order chaotic systems are frequency-domain method [14], Adomian decomposition method (ADM) [1] and Adams–Bashforth–Moulton (ABM) algorithm [68]. The frequency-domain method is not always reliable in detecting chaos behavior in nonlinear systems [70]. On the other hand, ABM and ADM are more accurate and convenient to analyze dynamical behaviors of a nonlinear system. Compared with the ABM, ADM yields more accurate results and needs less computing resources as well as memory resources [60]. Hence, the proposed FOHMCO system is implemented in FPGA by applying ADM scheme. The challenge of implementing the systems in FPGA is designing the fractional-order integrator which is not a readily available block in the System Generator [56–58]. As because the ADM algorithm converges fast [13], the first 6 terms are used to get the solution of FOHMCO system as in real cases, it is impossible to find the accurate value of x when t takes larger values [27]. Hence, we have to design a time discretization method. That is to say, for a time interval of t_i (initial time) to t_f (final time), we divide the interval into (t_n, t_{n+1}) and we get the value of $x(n+1)$ at time t_{n+1} by applying $x(n)$ at time t_n using the relation $x\,(n+1) = F\,(x\,(n))$ [27].

We use the ADM method [1,27] to discretize the fractional-order HMCO system for implementing in FPGA. The fractional-order discrete form of the dimensionless state equations for the FOHMCO system can be given as,

$$\begin{aligned} x_{n+1} &= \sum_{j=0}^{6} A_1^j \frac{h^{jq}}{\Gamma(jq+1)} \\ y_{n+1} &= \sum_{j=0}^{6} A_2^j \frac{h^{jq}}{\Gamma(jq+1)} \\ z_{n+1} &= \sum_{j=0}^{6} A_3^j \frac{h^{jq}}{\Gamma(jq+1)} \\ w_{n+1} &= \sum_{j=0}^{6} A_4^j \frac{h^{jq}}{\Gamma(jq+1)} \end{aligned} \tag{28}$$

where A_i^j are the Adomian polynomials with $i = 1, 2, 3, 4$ and $A_1^0 = x_n$, $A_2^0 = y_n$, $A_3^0 = z_n$, $A_4^0 = w_n$

The Adomian first polynomial is derived as,

$$\begin{aligned} A_1^1 &= A_2^0 + A_3^0 \\ A_2^1 &= cA_2^0 + dA_3^0 - aA_1^0 - bA_1^0\left(A_4^0\right)^2 \\ A_3^1 &= fA_2^0 + eA_3^0 - mA_1^0 - nA_1^0\left(A_4^0\right)^2 \\ A_4^1 &= A_1^0 \end{aligned} \tag{29}$$

The Adomian second polynomial is derived as,

$$\begin{aligned} A_1^2 &= A_2^1 + A_3^1 \\ A_2^2 &= cA_2^1 + dA_3^1 - aA_1^1 - b\left[A_1^1\left(A_4^0\right)^2 + A_1^0\left(A_4^1\right)^2\right] \\ A_3^2 &= fA_2^1 + eA_3^1 - mA_1^1 - n\left[A_1^1\left(A_4^0\right)^2 + A_1^0\left(A_4^1\right)^2\right] \\ A_4^2 &= A_1^1 \end{aligned} \tag{30}$$

The Adomian third polynomial is derived as,

$$\begin{aligned} A_1^3 &= A_2^2 + A_3^2 \\ A_2^3 &= cA_2^2 + dA_3^2 - aA_1^2 - b \\ &\quad \times\left[A_1^2\left(A_4^0\right)^2 + A_1^0\left(A_4^2\right)^2 + \frac{\Gamma(2q+1)}{\Gamma^2(q+1)}\left[A_2^1\left(A_4^1\right)^2\right]\right] \\ A_3^3 &= fA_2^2 + eA_3^2 - mA_1^2 - n \\ &\quad \times\left[A_1^2\left(A_4^0\right)^2 + A_1^0\left(A_4^2\right)^2 + \frac{\Gamma(2q+1)}{\Gamma^2(q+1)}\left[A_2^1\left(A_4^1\right)^2\right]\right] \\ A_4^3 &= A_1^2 \end{aligned} \tag{31}$$

The Adomian fourth polynomial is derived as,

$$\begin{aligned} A_1^4 &= A_2^3 + A_3^3 \\ A_2^4 &= cA_2^3 + dA_3^3 - aA_1^3 - b \\ &\quad \times\left[\begin{array}{l} A_1^3\left(A_4^0\right)^2 + A_1^0\left(A_4^3\right)^2 \\ +\frac{\Gamma(3q+1)}{\Gamma(q+1)\Gamma(2q+1)}\left[A_1^2\left(A_4^1\right)^2 + A_1^1\left(A_4^2\right)^2\right] \end{array}\right] \\ A_3^4 &= fA_2^3 + eA_3^3 - mA_1^3 - n \\ &\quad \times\left[\begin{array}{l} A_1^3\left(A_4^0\right)^2 + A_1^0\left(A_4^3\right)^2 \\ +\frac{\Gamma(3q+1)}{\Gamma(q+1)\Gamma(2q+1)}\left[A_1^2\left(A_4^1\right)^2 + A_1^1\left(A_4^2\right)^2\right] \end{array}\right] \\ A_4^4 &= A_1^3 \end{aligned} \tag{32}$$

The Adomian fifth polynomial is derived as,

$$\begin{aligned}
A_1^5 &= A_2^4 + A_3^4 \\
A_2^5 &= cA_2^4 + dA_3^4 - aA_1^4 - b \\
&\quad \times \left[\begin{array}{l} A_1^4 \left(A_4^0\right)^2 + A_1^0 \left(A_4^4\right)^2 \\ + \frac{\Gamma(4q+1)}{\Gamma(q+1)\Gamma(3q+1)} \left[A_1^3 \left(A_4^1\right)^2 + A_1^1 \left(A_4^3\right)^2 \right] \end{array} \right] \\
A_3^5 &= fA_2^4 + eA_3^4 - mA_1^4 - n \\
&\quad \times \left[\begin{array}{l} A_1^4 \left(A_4^0\right)^2 + A_1^0 \left(A_4^4\right)^2 \\ + \frac{\Gamma(4q+1)}{\Gamma(q+1)\Gamma(3q+1)} \left[A_1^3 \left(A_4^1\right)^2 + A_1^1 \left(A_4^3\right)^2 \right] \end{array} \right] \\
A_4^5 &= A_1^4
\end{aligned} \tag{33}$$

The Adomian sixth polynomial is derived as,

$$\begin{aligned}
A_1^6 &= A_2^5 + A_3^5 \\
A_2^6 &= cA_2^5 + dA_3^5 - aA_1^5 - b \\
&\quad \times \left[\begin{array}{l} A_1^5 \left(A_4^0\right)^2 + A_1^0 \left(A_4^5\right)^2 \\ + \frac{\Gamma(5q+1)}{\Gamma(q+1)\Gamma(4q+1)} \left[A_1^4 \left(A_4^1\right)^2 + A_1^1 \left(A_4^4\right)^2 \right] \end{array} \right] \\
A_3^6 &= fA_2^5 + eA_3^5 - mA_1^4 - n \\
&\quad \times \left[\begin{array}{l} A_1^5 \left(A_4^0\right)^2 + A_1^0 \left(A_4^5\right)^2 \\ + \frac{\Gamma(5q+1)}{\Gamma(q+1)\Gamma(4q+1)} \left[A_1^4 \left(A_4^1\right)^2 + A_1^1 \left(A_4^4\right)^2 \right] \end{array} \right] \\
A_4^6 &= A_1^5
\end{aligned} \tag{34}$$

where $h = t_{n+1} - t_n$ and $\Gamma(\bullet)$ is the gamma function. The fractional-order discretized system (28) is then implemented in FPGA and the necessary Adomian polynomials are calculated using (29)–(34). For implementing in FPGA, the value of h is taken as $0.001s$ and the initial conditions are fed into the forward register with fractional order taken as $q = 0.998$ for FOHMCO system. Figure 8 shows the RTL schematics of the FOHMCO system implemented in Kintex 7. Figure 9a shows the power consumed by FOHMCO system for order $q = 0.998$, and Fig. 9b shows the power consumed for various fractional orders and it can be seen that maximum power is consumed when the FOHMCO system exhibits the largest Lyapunov exponents. Table 1 shows the resources consumed with the consumed clock frequencies, and Fig. 10 shows the 2D phase portraits of the FPGA-implemented FOHMCO system.

7 Conclusion

A newly proposed memcapacitor hyperchaotic oscillator with infinite number of equilibrium points was investigated. Multistability observed and coexisting chaotic

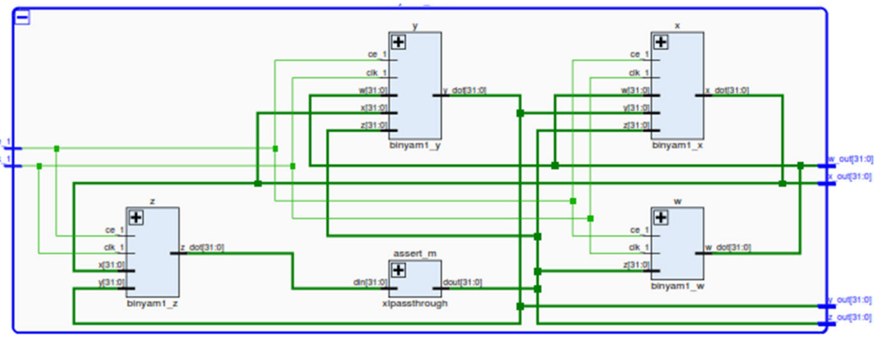

Fig. 8 RTL schematics of the FOHMCO system implemented in Kintex 7 (Device = 7k160t Package = fbg484 S). The sampling time of the system is kept at 0.01 s to minimize the time slack errors. The entire system is configured for a 32-bit operation

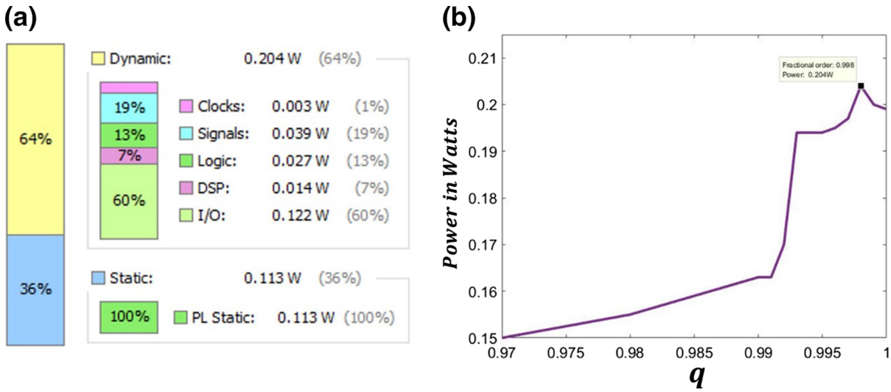

Fig. 9 **a** Power consumed by FOHMCO system for $q = 0.998$. **b** Power consumed by FOHMCO system for various fractional orders. It can be seen that maximum power of 0.204 W is consumed for order $q = 0.998$ when the FOHMCO system shows positive largest Lyapunov exponent

Table 1 Resource consumption of FPGA-implemented FOHMCO system

Resource	Utilization	Available (MHZ)	Utilization %	Clock frequency	
				Available	Used (MHZ)
LUT	1763	101400	1.74	500	260
FF	256	202800	0.13	500	207
DSP	16	600	2.67	250	104
IO	129	285	45.26	300	115
BUFG	1	32	3.13	300	87

oscillators were found. Dynamical analysis showed the existence of chaotic and hyperchaotic oscillators for various parameter values. The fractional-order model of the proposed hyperchaotic oscillator was derived and analyzed. Finally, the fractional-

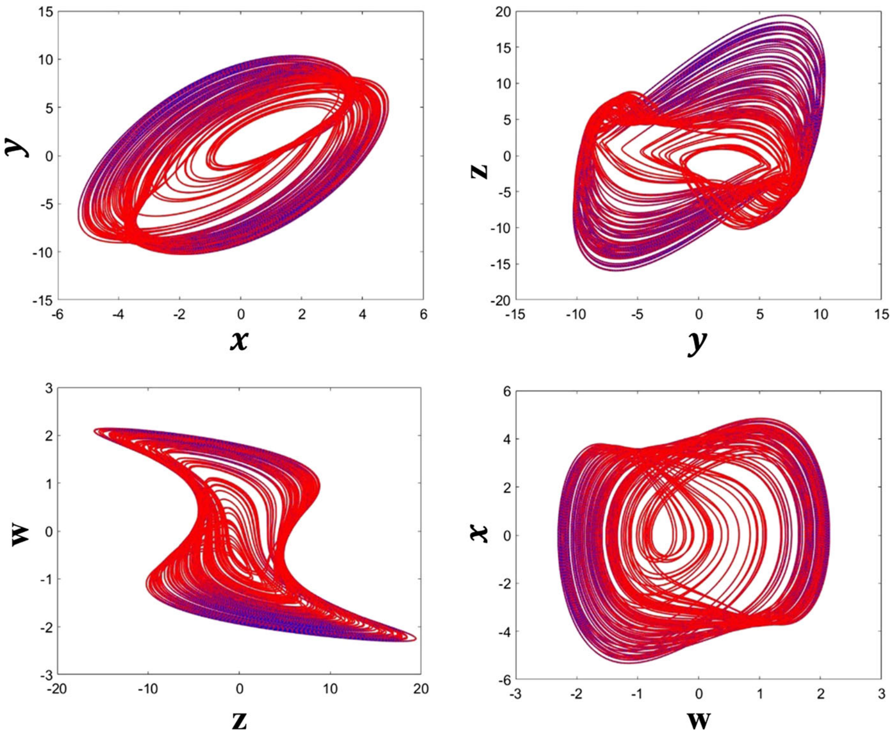

Fig. 10 2D phase portraits of the FPGA-implemented FOHMCO system. The initial conditions and parameter values are taken as in Sect. 2, and the order of the system is $q = 0.998$

order model was implemented by FPGA and resource and power consumption details for various fractional orders were presented.

References

1. G. Adomian, A review of the decomposition method and some recent results for nonlinear equations. Math. Comput. Model. **13**(7), 17–43 (1990)
2. M.P. Aghababa, Robust finite-time stabilization of fractional-order chaotic systems based on fractional Lyapunov stability theory. J. Comput. Nonlinear Dyn. **7**(2), 021010 (2012)
3. D. Baleanu, K. Diethelm, E. Scalas, J.J. Trujillo, *Fractional Calculus: Models and Numerical Methods*, vol. 5 (World Scientific, Singapore, 2016)
4. K. Barati, S. Jafari, J.C. Sprott, V.-T. Pham, Simple chaotic flows with a curve of equilibria. Int. J. Bifurc. Chaos **26**(12), 1630034 (2016)
5. R. Barboza, L.O. Chua, The four-element Chua's circuit. Int. J. Bifurc. Chaos **18**(04), 943–955 (2008)
6. G. Bianchi, N. Kuznetsov, G. Leonov, M. Yuldashev, R. Yuldashev: Limitations of PLL simulation: hidden oscillations in MatLab and SPICE, in *Ultra Modern Telecommunications and Control Systems and Workshops (ICUMT), 2015 7th International Congress on 2015* (IEEE), pp. 79–84
7. B. Błażejczyk-Okolewska, T. Kapitaniak, Co-existing attractors of impact oscillator. Chaos Solitons Fractals **9**(8), 1439–1443 (1998)
8. B. Bo-Cheng, S. GuoDong, X. JianPing, L. Zhong, P. SaiHu, Dynamics analysis of chaotic circuit with two memristors. Sci. China Technol. Sci. **54**(8), 2180–2187 (2011). https://doi.org/10.1007/s11431-011-4400-6

9. E.A. Boroujeni, H.R. Momeni, Non-fragile nonlinear fractional order observer design for a class of nonlinear fractional order systems. Sig. Process. **92**(10), 2365–2370 (2012)
10. A. Buscarino, L. Fortuna, M. Frasca, L.V. Gambuzza, A gallery of chaotic oscillators based on HP memristor. Int. J. Bifurc. Chaos **23**(05), 1330015 (2013)
11. A. Buscarino, L. Fortuna, M. Frasca, L. Valentina Gambuzza, A chaotic circuit based on Hewlett–Packard memristor. Chaos Interdiscip. J. Nonlinear Sci. **22**(2), 023136 (2012)
12. D. Cafagna, G. Grassi, Fractional-order systems without equilibria: the first example of hyperchaos and its application to synchronization. Chin. Phys. B **24**(8), 080502 (2015)
13. R. Caponetto, S. Fazzino, An application of Adomian decomposition for analysis of fractional-order chaotic systems. Int. J. Bifurc. Chaos **23**(03), 1350050 (2013)
14. A. Charef, H. Sun, Y. Tsao, B. Onaral, Fractal system as represented by singularity function. IEEE Trans. Autom. Control **37**(9), 1465–1470 (1992)
15. L. Chua, Memristor-the missing circuit element. IEEE Trans. Circuit Theory **18**(5), 507–519 (1971)
16. L.O. Chua, S.M. Kang, Memristive devices and systems. Proc. IEEE **64**(2), 209–223 (1976)
17. A. Chudzik, P. Perlikowski, A. Stefanski, T. Kapitaniak, Multistability and rare attractors in van der Pol–Duffing oscillator. Int. J. Bifurc. Chaos **21**(07), 1907–1912 (2011)
18. F. Corinto, V. Krulikovskyi, S.D. Haliuk: Memristor-based chaotic circuit for pseudo-random sequence generators, in 2016 *18th Mediterranean 2016 Electrotechnical Conference (MELECON)* (IEEE), pp. 1–3
19. M.-F. Danca, N. Kuznetsov, Hidden chaotic sets in a Hopfield neural system. Chaos Solitons Fractals **103**, 144–150 (2017)
20. M.-F. Danca, N. Kuznetsov, G. Chen, Unusual dynamics and hidden attractors of the Rabinovich–Fabrikant system. Nonlinear Dyn. **88**(1), 791–805 (2017)
21. M.-F. Danca, W.K. Tang, G. Chen, Suppressing chaos in a simplest autonomous memristor-based circuit of fractional order by periodic impulses. Chaos Solitons Fractals **84**, 31–40 (2016)
22. K. Diethelm, *The Analysis of Fractional Differential Equations: An Application-Oriented Exposition Using Differential Operators of Caputo Type* (Springer, Berlin, 2010)
23. E. Dong, Z. Liang, S. Du, Z. Chen, Topological horseshoe analysis on a four-wing chaotic attractor and its FPGA implement. Nonlinear Dyn. **83**(1–2), 623–630 (2016)
24. D. Dudkowski, S. Jafari, T. Kapitaniak, N.V. Kuznetsov, G.A. Leonov, A. Prasad, Hidden attractors in dynamical systems. Phys. Rep. **637**, 1–50 (2016). https://doi.org/10.1016/j.physrep.2016.05.002
25. S. Ellner, A.R. Gallant, D. McCaffrey, D. Nychka, Convergence rates and data requirements for Jacobian-based estimates of Lyapunov exponents from data. Phys. Lett. A **153**(6–7), 357–363 (1991)
26. A.L. Fitch, H.H. Iu, D. Yu: Chaos in a memcapacitor based circuit, in *2014 IEEE International Symposium on 2014 Circuits and Systems (ISCAS)* (IEEE), pp. 482–485
27. S. He, K. Sun, H. Wang, Complexity analysis and DSP implementation of the fractional-order lorenz hyperchaotic system. Entropy **17**(12), 8299–8311 (2015)
28. S. Jafari, V.-T. Pham, T. Kapitaniak, Multiscroll chaotic sea obtained from a simple 3D system without equilibrium. Int. J. Bifurc. Chaos **26**(02), 1650031 (2016)
29. S. Jafari, J.C. Sprott, Erratum to:"Simple chaotic flows with a line equilibrium" [Chaos, Solitons and Fractals 57 (2013) 79–84]. Chaos Solitons Fractals **77**, 341–342 (2015)
30. S. Jafari, J.C. Sprott, Simple chaotic flows with a line equilibrium. Chaos Solitons Fractals **57**, 79–84 (2013)
31. P. Jaros, L. Borkowski, B. Witkowski, K. Czolczynski, T. Kapitaniak, Multi-headed chimera states in coupled pendula. Eur. Phys. J. Spec. Top. **224**(8), 1605–1617 (2015)
32. H. Kim, M.P. Sah, C. Yang, S. Cho, L.O. Chua, Memristor emulator for memristor circuit applications. IEEE Trans. Circuits Syst. I Regul. Pap. **59**(10), 2422–2431 (2012)
33. S.T. Kingni, V.-T. Pham, S. Jafari, G.R. Kol, P. Woafo, Three-dimensional chaotic autonomous system with a circular equilibrium: analysis, circuit implementation and its fractional-order form. Circuits Syst. Signal Process. **35**(6), 1933–1948 (2016)
34. N. Kuznetsov, The Lyapunov dimension and its estimation via the Leonov method. Phys. Lett. A **380**(25), 2142–2149 (2016)
35. N. Kuznetsov, T. Alexeeva, G. Leonov: Invariance of Lyapunov characteristic exponents, Lyapunov exponents, and Lyapunov dimension for regular and non-regular linearizations. arXiv preprint arXiv:1410.2016 (2014)

36. N. Kuznetsov, G. Leonov, M. Yuldashev, R. Yuldashev, Hidden attractors in dynamical models of phase-locked loop circuits: limitations of simulation in MATLAB and SPICE. Commun. Nonlinear Sci. Numer. Simul. **51**, 39–49 (2017)
37. N. Kuznetsov, T. Mokaev, P. Vasilyev, Numerical justification of Leonov conjecture on Lyapunov dimension of Rossler attractor. Commun. Nonlinear Sci. Numer. Simul. **19**(4), 1027–1034 (2014)
38. V. Lakshmikantham, A. Vatsala, Basic theory of fractional differential equations. Nonlinear Anal. Theory Methods Appl. **69**(8), 2677–2682 (2008)
39. D.M. Leenaerts, Higher-order spectral analysis to detect power-frequency mechanisms in a driven Chua's circuit. Int. J. Bifurc. Chaos **7**(06), 1431–1440 (1997)
40. G.A. Leonov, N.V. Kuznetsov, Hidden attractors in dynamical systems. From hidden oscillations in Hilbert–Kolmogorov, Aizerman, and Kalman problems to hidden chaotic attractor in Chua circuits. Int. J. Bifurc. Chaos **23**(01), 1330002 (2013)
41. C. Li, Z. Gong, D. Qian, Y. Chen, On the bound of the Lyapunov exponents for the fractional differential systems. Chaos Interdisc. J. Nonlinear Sci. **20**(1), 013127 (2010)
42. C. Li, W. Hu, J.C. Sprott, X. Wang, Multistability in symmetric chaotic systems. Eur. Phys. J. Spec. Top. **224**(8), 1493–1506 (2015)
43. R. Li, W. Chen, Fractional order systems without equilibria. Chin. Phys. B **22**, 040503 (2013)
44. Y. Maistrenko, T. Kapitaniak, P. Szuminski, Locally and globally riddled basins in two coupled piecewise-linear maps. Phys. Rev. E **56**(6), 6393 (1997)
45. A. Maus, J. Sprott, Evaluating Lyapunov exponent spectra with neural networks. Chaos Solitons Fractals **51**, 13–21 (2013)
46. B. Muthuswamy, Implementing memristor based chaotic circuits. Int. J. Bifurc. Chaos **20**(05), 1335–1350 (2010)
47. B. Muthuswamy, P.P. Kokate, Memristor-based chaotic circuits. IETE Tech. Rev. **26**(6), 417–429 (2009)
48. Y.V. Pershin, M. Di Ventra, Emulation of floating memcapacitors and meminductors using current conveyors. Electron. Lett. **47**(4), 243–244 (2011)
49. I. Petráš, Method for simulation of the fractional order chaotic systems. Acta Montan. Slovaca **11**(4), 273–277 (2006)
50. C. Pezeshki, S. Elgar, R. Krishna, Bispectral analysis of possessing chaotic motion. J. Sound Vib. **137**(3), 357–368 (1990)
51. V.-T. Pham, S. Jafari, T. Kapitaniak, Constructing a chaotic system with an infinite number of equilibrium points. Int. J. Bifurc. Chaos **26**(13), 1650225 (2016)
52. V.T. Pham, S. Jafari, C. Volos, T. Kapitaniak, A gallery of chaotic systems with an infinite number of equilibrium points. Chaos Solitons Fractals **93**, 58–63 (2016)
53. C. Pradhan, S.K. Jena, S.R. Nadar, N. Pradhan, Higher-order spectrum in understanding nonlinearity in EEG rhythms. Comput. Math. Methods Med. **2012**, 206857 (2012). https://doi.org/10.1155/2012/206857
54. H. Qing-Hui, L. Zhi-Jun, Z. Jin-Fang, Z. Yi-Cheng, Design and simulation of a memristor chaotic circuit based on current feedback op amp. Acta. Phys. Sin. (Chinese Edition) **63**(18) (2014). https://doi.org/10.7498/aps.63.180502
55. K. Rajagopal, L. Guessas, A. Karthikeyan, A. Srinivasan, G. Adam, Fractional order memristor no equilibrium chaotic system with its adaptive sliding mode synchronization and genetically optimized fractional order PID synchronization. Complexity **2017**, 1892618 (2017). https://doi.org/10.1155/2017/1892618
56. K. Rajagopal, L. Guessas, S. Vaidyanathan, A. Karthikeyan, A. Srinivasan, Dynamical analysis and FPGA implementation of a novel hyperchaotic system and its synchronization using Adaptive Sliding mode control and genetically optimized PID control. Math. Prob. Eng. **2017**, 7307452 (2017). https://doi.org/10.1155/2017/7307452
57. K. Rajagopal, A. Karthikeyan, P. Duraisamy, Hyperchaotic Chameleon: fractional order FPGA mentation. Complexity **2017**, 8979408 (2017). https://doi.org/10.1155/2017/8979408
58. K. Rajagopal, A. Karthikeyan, A.K. Srinivasan, FPGA implementation of novel fractional-order chaotic systems with two equilibriums and no equilibrium and its adaptive sliding mode synchronization. Nonlinear Dyn. **87**, 1–24 (2017)
59. V. Rashtchi, M. Nourazar, FPGA Implementation of a real-time weak signal detector using a duffing oscillator. Circuits Syst. Signal Process. **34**(10), 3101–3119 (2015)

60. H. Shao-Bo, S. Ke-Hui, W. Hui-Hai, Solution of the fractional-order chaotic system based on Adomian decomposition algorithm and its complexity analysis. Acta Phys. Sin. (Chinese Edition) **63**(3) (2014). https://doi.org/10.7498/aps.63.030502
61. P. Sharma, M. Shrimali, A. Prasad, N. Kuznetsov, G. Leonov, Control of multistability in hidden attractors. Eur. Phys. J. Spec. Top. **224**(8), 1485–1491 (2015)
62. A. Silchenko, T. Kapitaniak, V. Anishchenko, Noise-enhanced phase locking in a stochastic bistable system driven by a chaotic signal. Phys. Rev. E **59**(2), 1593 (1999)
63. J.C. Sprott, A proposed standard for the publication of new chaotic systems. Int. J. Bifurc. Chaos **21**(09), 2391–2394 (2011)
64. J.C. Sprott, C. Li, Asymmetric bistability in the Rössler system. Acta Phys. Pol. B **32**, 97–107 (2017)
65. J.C. Sprott, X. Wang, G. Chen, Coexistence of point, periodic and strange attractors. Int. J. Bifurc. Chaos **23**(05), 1350093 (2013)
66. A. Stefanski, A. Dabrowski, T. Kapitaniak, Evaluation of the largest Lyapunov exponent in dynamical systems with time delay. Chaos Solitons Fractals **23**(5), 1651–1659 (2005)
67. D.B. Strukov, G.S. Snider, D.R. Stewart, R.S. Williams, The missing memristor found. Nature **453**(7191), 80–83 (2008)
68. H. Sun, A. Abdelwahab, B. Onaral, Linear approximation of transfer function with a pole of fractional power. IEEE Trans. Autom. Control **29**(5), 441–444 (1984)
69. F.R. Tahir, S. Jafari, V.-T. Pham, C. Volos, X. Wang, A novel no-equilibrium chaotic system with multiwing butterfly attractors. Int. J. Bifurc. Chaos **25**(04), 1550056 (2015)
70. M. Tavazoei, M. Haeri, Unreliability of frequency-domain approximation in recognising chaos in fractional-order systems. IET Signal Proc. **1**(4), 171–181 (2007)
71. E. Tlelo-Cuautle, V. Carbajal-Gomez, P. Obeso-Rodelo, J. Rangel-Magdaleno, J.C. Nuñez-Perez, FPGA realization of a chaotic communication system applied to image processing. Nonlinear Dyn. **82**(4), 1879–1892 (2015)
72. E. Tlelo-Cuautle, A. Pano-Azucena, J. Rangel-Magdaleno, V. Carbajal-Gomez, G. Rodriguez-Gomez, Generating a 50-scroll chaotic attractor at 66 MHz by using FPGAs. Nonlinear Dyn. **85**(4), 2143–2157 (2016)
73. E. Tlelo-Cuautle, J. Rangel-Magdaleno, A. Pano-Azucena, P. Obeso-Rodelo, J.C. Nuñez-Perez, FPGA realization of multi-scroll chaotic oscillators. Commun. Nonlinear Sci. Numer. Simul. **27**(1), 66–80 (2015)
74. Z. Trzaska: Matlab solutions of chaotic fractional order circuits. Chapter 19, in All Assi. Engineering Education and Research Using MATLAB. Intech, Rijeka (2011)
75. G.-Y. Wang, P.-P. Jin, X.-W. Wang, Y.-R. Shen, F. Yuan, X.-Y. Wang, A flux-controlled model of meminductor and its application in chaotic oscillator. Chin. Phys. B **25**(9), 090502 (2016)
76. G. Wang, M. Cui, B. Cai, X. Wang, T. Hu, A chaotic oscillator based on HP memristor model. Math. Probl. Eng. **2015**, 561901 (2015). https://doi.org/10.1155/2015/561901
77. G. Wang, S. Jiang, X. Wang, Y. Shen, F. Yuan, A novel memcapacitor model and its application for generating chaos. Math. Probl. Eng. **2016**, 3173696 (2016). https://doi.org/10.1155/2016/3173696
78. G. Wang, C. Shi, X. Wang, F. Yuan, Coexisting oscillation and extreme multistability for a memcapacitor-based circuit. Math. Prob. Eng. **2017**, 6504969 (2017). https://doi.org/10.1155/2017/6504969
79. Q. Wang, S. Yu, C. Li, J. Lü, X. Fang, C. Guyeux, J.M. Bahi, Theoretical design and FPGA-based implementation of higher-dimensional digital chaotic systems. IEEE Trans. Circuits Syst. I Regul. Pap. **63**(3), 401–412 (2016)
80. A. Wolf, J.B. Swift, H.L. Swinney, J.A. Vastano, Determining Lyapunov exponents from a time series. Physica D **16**(3), 285–317 (1985)
81. X. Ya-Ming, W. Li-Dan, D. Shu-KaiL, A memristor-based chaotic system and its field programmable gate array implementation. ACTA Phys. Sin. **65**(12), 120503 (2016). https://doi.org/10.7498/aps.65.120503
82. C. Yang, Q. Hu, Y. Yu, R. Zhang, Y. Yao, J. Cai: Memristor-based chaotic circuit for text/image encryption and decryption, in *2015 8th International Symposium on 2015 Computational Intelligence and Design (ISCID)* (IEEE), pp. 447–450
83. D. Yu, Y. Liang, H. Chen, H.H. Iu, Design of a practical memcapacitor emulator without grounded restriction. IEEE Trans. Circuits Syst. II Express Briefs **60**(4), 207–211 (2013)
84. R. Zhang, J. Gong, Synchronization of the fractional-order chaotic system via adaptive observer. Syst. Sci. Control Eng. Open Access J. **2**(1), 751–754 (2014)